Appl. Phys. A (2016) 122:725
DOI 10.1007/s00339-016-0259-5

Applied Physics A
Materials Science & Processing

Structure and optical absorption properties of $NiTiO_3$ nanocrystallites

Ming-Wei Li[1,2] · Jin-Pei Yuan[1,2] · Xiao-Mei Gao[1] · Er-Qian Liang[1,2] · Cheng-Yang Wang[2,3]

Received: 25 March 2016 / Accepted: 5 July 2016 / Published online: 8 July 2016

Abstract Nickel titanate ($NiTiO_3$) nanocrystallites are synthesized via a solid-state reaction from a precursor prepared by a homogeneous precipitation method. Ilmenite-structural $NiTiO_3$ consists of alternating layers of NiO_6 and TiO_6 octahedra. It not only strongly absorbs ultraviolet light (wavelength <360 nm) but also selectively absorbs visible light mainly in a wavelength range of 420–540 nm and above 700 nm. The synthetic $NiTiO_3$ is a direct-gap semiconducting material with a band gap of 3.00 eV and has obvious absorbance peaks at 448, 502, and 743 nm, corresponding to the photon energies of 2.77, 2.47, and 1.67 eV, respectively. Nevertheless, $NiTiO_3$ does not exhibit obvious photocatalytic activity in the degradation of methylene blue in water. It is proposed that the visible light absorbance peaks of $NiTiO_3$ mainly originate from the Ni: $d \rightarrow d$ charge-transfer transitions within its valence band. $NiTiO_3$ has wide energy gaps from the hybridized Ni 3*d* and O 2*p* orbitals to the Ti 3*d* orbitals, which block both $Ni^{2+} \rightarrow Ti^{4+}$ and $O^{2-} \rightarrow Ti^{4+}$ charge-transfer transitions between valence band and conduction band, and thus baffle its photocatalytic performance.

✉ Ming-Wei Li
mingweili@tju.edu.cn

[1] Department of Chemistry, Tianjin University, Tianjin 300072, China

[2] Key Laboratory for Green Chemical Technology of Ministry of Education, School of Chemical Engineering and Technology, Tianjin University, Tianjin 300072, China

[3] Collaborative Innovation Center of Chemical Science and Engineering (Tianjin), Tianjin University, Tianjin 300072, China

1 Introduction

Nickel titanate ($NiTiO_3$) is an ilmenite-structural *n*-type semiconducting material with particular magnetic, electric, and optical properties [1–8]. It exhibits both semiconducting and magnetic behaviors and could be exploited for applications including microwave devices and varistors [8]. Besides applied as yellow pigments in ceramics or automobile industry [9–13], $NiTiO_3$ is widely studied as a photocatalyst [14–25]. Although there still are arguments about its band gaps including 2.12 eV [2], 3.18 eV [3], 2.8 eV [17], 3.0–3.1 eV [4, 15, 16, 18, 20], and 3.2 eV [8], many researchers consider that $NiTiO_3$ possesses narrower band gaps resulted from $Ni^{2+} \rightarrow Ti^{4+}$ charge-transfer transitions than TiO_2 (3.3 eV for anatase, and 3.1 eV for rutile [26]) caused by $O^{2-} \rightarrow Ti^{4+}$ transitions and then has visible light photocatalytic activity. Asahi et al. [27] reported that yellow nitrogen-doped TiO_2 has a narrowed band gap and exhibits optical absorption and photocatalytic activity under visible light (wavelength <500 nm). They suggested that the doped nitrogen has substituted partial oxygen, and the consequential transition N $2p \rightarrow$ Ti $3d$ instead of O $2p \rightarrow$ Ti $3d$ makes a redshift of the absorption edge of $TiO_{2-x}N_x$. It is interesting to investigate the optical absorption and photocatalytic activity of $NiTiO_3$, which are important for its applications in paints or cosmetics.

In this work, we synthesized $NiTiO_3$ nanocrystallites by a homogeneous precipitation method and investigated their optical absorption properties. To synthesize $NiTiO_3$ nanocrystallites, most researchers prepared precursors by wet chemical methods and then calcined the precursors to form nano-sized $NiTiO_3$ crystallites. The precursors could be prepared by several methods, including chemical co-precipitation method [3, 10], sol–gel method [5, 8, 24],

polymeric precursor method [4, 28], etc. The homogeneous precipitation method has ever been used to synthesize well-ordered crystallites including $NiTiO_3$ [18, 29, 30]. During the process, the mixed Ti- and Ni-containing precipitate gradually forms along with the hydrolysis of urea. Hence, the well-mixed precursor more easily forms well-ordered $NiTiO_3$ crystallites.

The investigation reveals the synthetic $NiTiO_3$ nanocrystallites having a band gap of 3.00 eV, and obviously, selectively absorbing visible light with certain wavelength. Comparing the optical absorption properties and the band structures of TiO_2, NiO, and $NiTiO_3$, we propose that the wide energy gap from the hybridized Ni 3*d* and O 2*p* orbitals to the Ti 3*d* orbitals baffles the photocatalytic performance of $NiTiO_3$.

2 Experimental

2.1 Synthesis of $NiTiO_3$ nanocrystallites

Stoichiometric $TiCl_4$ in a hydrochloric acid solution and $Ni(NO_3)_2{\cdot}6H_2O$ were dissolved in deionized water under vigorous stirring. Urea was added into the solution as precipitator to gradually form a Ti- and Ni-containing precipitate. The gradually thickening suspension was filtered after being stirred for 6 h at the refluxing temperature. The green filter cake was, respectively, washed with deionized water and anhydrous ethanol and dried in air overnight at 130 °C to form the dried precursor of $NiTiO_3$. After being ground, the precursor was annealed in air heated at 800 °C for 6 h and finally formed a yellow product.

2.2 Characterization

The dried precursor was analyzed by thermogravimetric analysis and differential scanning calorimetry (TG–DSC, STA 409 PC/PG, NETZSCH) from room temperature to 1100 °C in air flow. The synthetic powder was characterized by a power X-ray diffractometer (XRD, D/MAX 2500 V/PC, Rigaku) using Cu Kα radiation ($\lambda = 0.15406$ nm). Its mean crystal size was calculated by the Scherrer formula. The powder is a mixture of $NiTiO_3$, rutile, and anatase phases. So their weight fractions were, respectively, calculated by following formulas [31]:

$$W_{NT} = K_{NT}I_{NT}/(K_A + I_R + K_{NT}I_{NT})$$

$$W_R = I_R/(K_A + I_R + K_{NT}I_{NT})$$

$$W_A = K_A I_A/(K_A + I_R + K_{NT}I_{NT})$$

where W_{NT}, W_R, and W_A are the weight fractions of $NiTiO_3$, rutile, and anatase, respectively. I_{NT}, I_R, and I_A, respectively, represent the intensities of main diffraction peaks of $NiTiO_3$ (104), rutile (110), and anatase (101). K_{NT} (= 2.60), K_R (= 3.68), and K_A (= 5.05) are the reference intensity ratios of the three phases, and are, respectively, selected from JCPDS 76-0334, 84-1284, and 84-1286. The sample's microstructures were detected by a field-emission high-resolution transmission electron microscope (HRTEM, Tecnai G^2 F20, FEI) with an energy-dispersive X-ray spectroscope (EDX). The samples' ultraviolet–visible light diffuse reflectance spectra (UV–Vis DRS) were measured by a JASCO V-570 spectrometer in a wavelength range of 200–800 nm at room temperature. A commercial TiO_2 (P-25, Degussa) was used as reference.

The samples' photocatalytic performance was estimated by measuring the decomposition rates of methylene blue (40 mg) in an aqueous solution (400 ml) with catalyst powder (200 mg). The reactor was equipped with cooling water circulating between inner and outer quartz tubes to keep the reaction at ~30 °C. The mixed methylene blue solution and catalyst powder in the outer tubes were vigorously stirred for 30 min to equably disperse the catalyst powder before irradiation. Air was pumped into the reactor to degrade methylene blue. A 300-W high-pressure mercury arc lamp placed in the inner quartz tube was used as light source. A blank sample without a catalyst was carried out following the same procedure. After the photolysis, the remaining methylene blue concentrations in the aqueous solutions were detected by measuring the absorbance at 665 nm using a HP8453 UV–Vis spectrophotometer.

3 Result and discussion

Figure 1 shows the TG–DSC curves of the precursor of $NiTiO_3$. The precursor loses ~14.4 % weight from room temperature to 800 °C. The endothermic peak at 100 °C is attributed to the escape of surface water. The exothermic phenomenon above 800 °C is caused by the descending formation enthalpy of $NiTiO_3$ with increasing temperature [32]. According to the results, 800 °C was selected as the reaction temperature.

Figure 2a shows XRD pattern of the synthetic powder. It is a mixture of $NiTiO_3$, rutile, and anatase with a weight ratio of 69/22/9. The mean crystal sizes of $NiTiO_3$, rutile, and anatase are 40, 42, and 25 nm, respectively. Most TiO_2 exists in a rutile phase. It is accepted that the rutile phase is more stable than the anatase phase at high temperature. No other distinct Ni-containing compounds, such as NiO, were detected. It means that almost all Ni had been utilized to form $NiTiO_3$ nanocrystallites. During the synthesis of $NiTiO_3$, the raw materials contain equimolar Ti^{4+} and Ni^{2+} ions, but more Ni^{2+} ions lost due to the higher solubility of Ni-containing precipitate and the filtering and washing

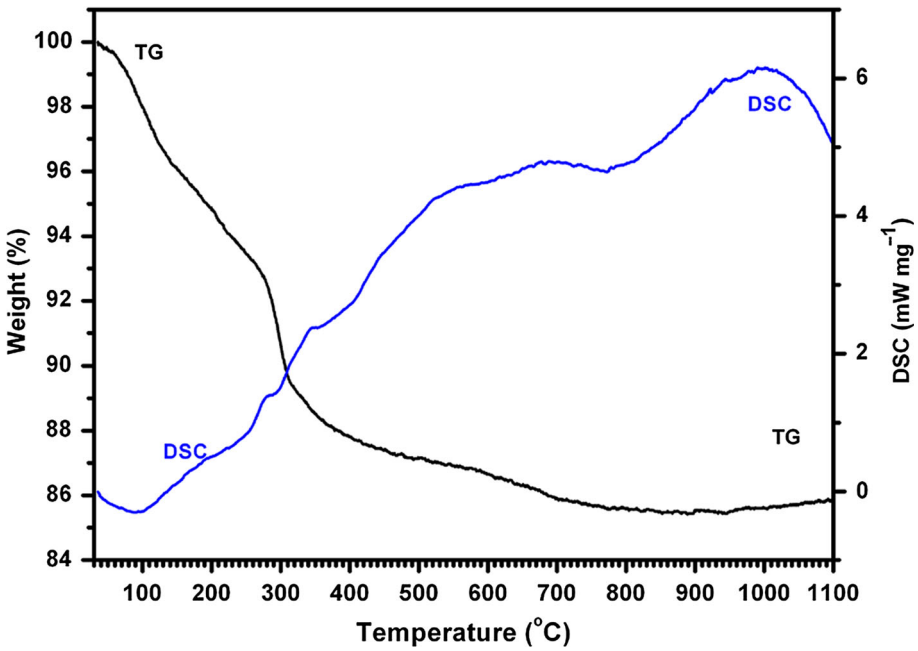

Fig. 1 TG–DSC *curves* of the precursor of $NiTiO_3$

processes. The product hardly keeps the same metal ratios with that in raw materials by a homogeneous precipitation method. The similar problem exists in the conventional chemical co-precipitation method.

The lattice parameters of the synthetic $NiTiO_3$ are $R\bar{3}$, $a = 5.0290(3)$ Å, $c = 13.7895(2)$ Å, $V = 302.03$ Å^3, $Z = 6$, and $D_x = 5.0998$ g cm^{-3}. They consist with the reported data of $NiTiO_3$ in literature [8, 25, 28, 37] and the JCPDS 33-0960. The rhombohedral unit cell of $NiTiO_3$ is illustrated in Fig. 2b. The alternating layers of Ni and Ti atoms are perpendicular to the *c* axes. The O atoms between the transition metal layers are octahedrally coordinated with the centered Ni or Ti atoms.

Figure 3a presents the nanosized particles agglomerate together. Figure 3b is an enlarged image and exhibits the particles' crystal structures. There are different lattice spaces of 0.25 and 0.35 nm, respectively, corresponding to the (110) layers of $NiTiO_3$ and (101) layers of rutile. An EDX spectrum indicates that the ratio of Ni/Ti/O in a selected small area is 18.9/20.2/60.9, namely $Ni_{0.93}Ti_{1.00}O_3$. So the selected area almost contains $NiTiO_3$.

Figure 4a shows the samples' UV–Vis DRS. Degussa P-25 strongly absorbs UV light (wavelength <320 nm) and has an absorption edge of ~410 nm. It hardly selectively absorbs visible light. As comparison, the synthetic powder shows a redshift for its UV absorption edge. Its absorbance in visible light region is mainly caused by $NiTiO_3$ because the doped TiO_2 hardly absorbs visible light [32]. $NiTiO_3$ not only strongly absorbs UV light (<360 nm) but also selectively absorbs visible light mainly within 420–540 nm and above 700 nm. It shows the absorbance peaks at 448, 502, and 743 nm, which correspond to the photon energies of 2.77, 2.47, and 1.67 eV, respectively. The high visible light absorbance centered at 448 nm (violet color) and 743 nm (red color) make $NiTiO_3$ showing the complementary colors of yellow and green.

The band gap of $NiTiO_3$ is estimated by the Tauc plot [15, 34, 35], namely the curve of $(\alpha hv)^{2/n}$ versus hv. The α and hv, respectively, are the absorbance and photon energy. The n value indicates the transitions from the valence band (VB) to the conduction band (CB) being direct ($n = 1$) or indirect ($n = 4$). The hv value at the intersection point of the tangent and the horizontal axis is the band gap energy.

As shown in Fig. 4b, the calculation results indicate that either $NiTiO_3$ or Degussa P-25 has a direct band gap. The band gap of Degussa P-25 is ~3.32 eV, which coincides with the band gap of anatase TiO_2. $NiTiO_3$ has a narrower band gap of 3.00 eV.

The photocatalytic performance of $NiTiO_3$ and Degussa P-25 is evaluated by degrading methylene blue. Figure 5 shows that all methylene blue had been degraded by Degussa P-25 in 20 min. But, $NiTiO_3$ exhibits rather low photocatalytic activity. Only 10 % methylene blue degraded in 80 min. The results approve the viewpoint of Goodenough et al. [15]. They predicted that the geometry of $NiTiO_3$ makes the oscillator strength for $Ni^{2+} \rightarrow Ti^{4+}$ charge-transfer too weak to have an acceptable response to visible light.

The optical and photocatalytic properties of $NiTiO_3$ are closely related with its crystal size, crystal structure, and band structure. Both experimental and theoretic results present the redshifts of UV light absorption edges for

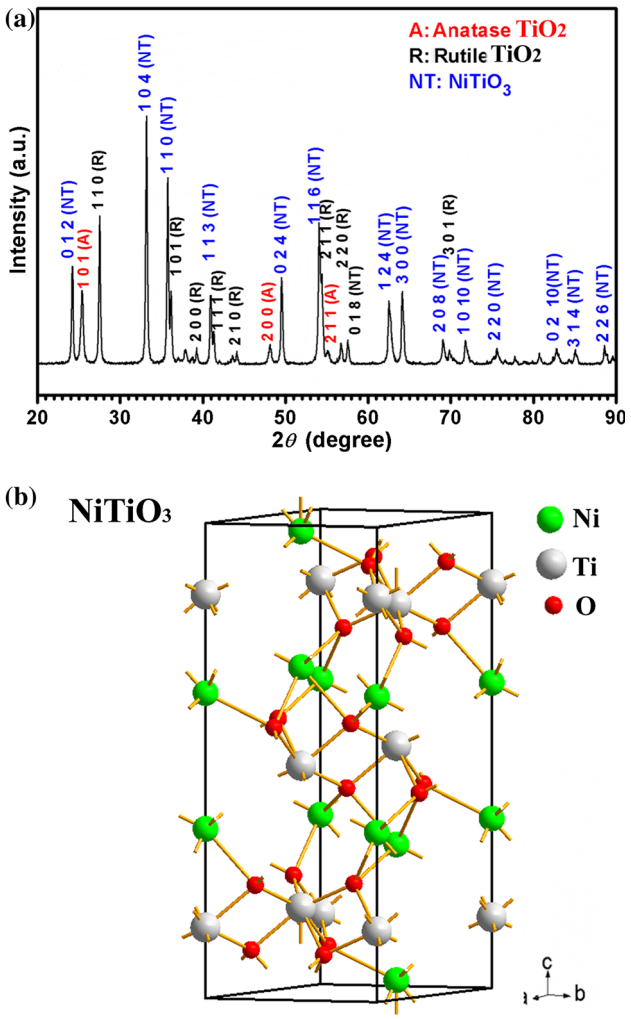

Fig. 2 **a** XRD pattern of the synthetic $NiTiO_3$-contained powder and **b** the unit cell of $NiTiO_3$

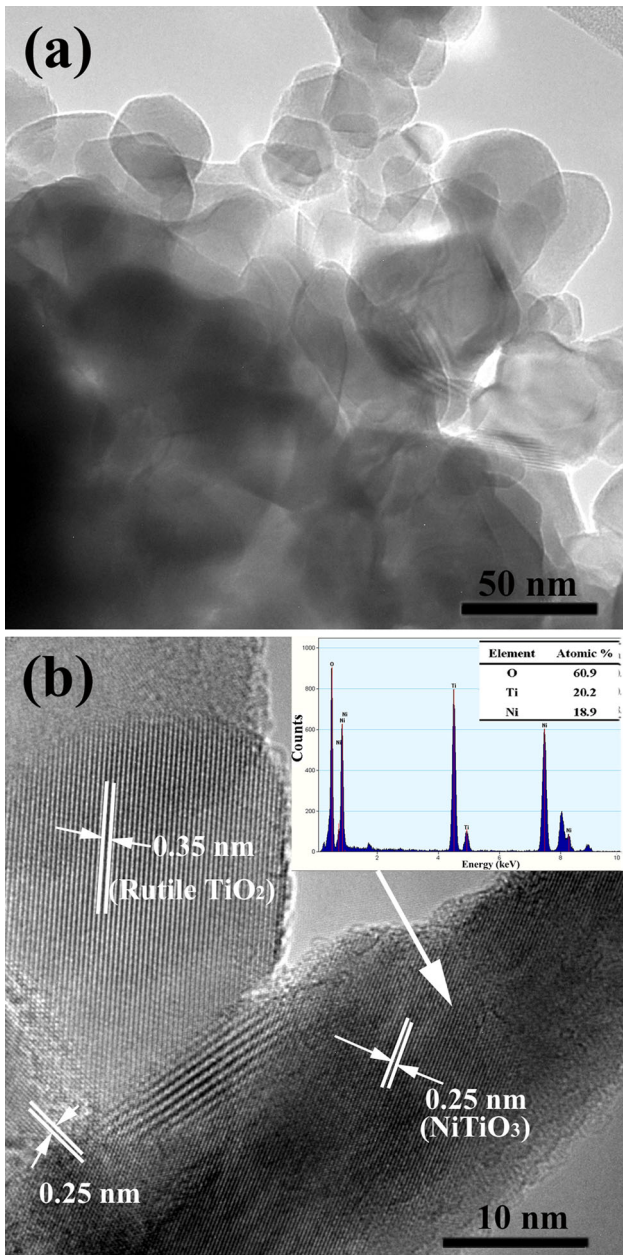

Fig. 3 HRTEM images of the synthetic powder. The *inset* in **b** is an EDX spectrum of the selected area

nanosized $NiTiO_3$ [3, 7, 19, 23, 33, 36–38]. Nevertheless, $NiTiO_3$ often has absorption peaks near 448, 502, and 745 nm, which almost do not shift with the size of $NiTiO_3$ crystallites [3, 7, 9, 18, 19, 23, 33, 38]. Its yellow color also indicates $NiTiO_3$ selectively absorbs visible light. However, the absorbed visible light did not obviously improve the photocatalytic performance of $NiTiO_3$ in this work.

To understand the optical absorption properties of $NiTiO_3$, we simply compare the energy band structures and density of states (DOSs) of TiO_2, NiO, and $NiTiO_3$ based on recent reports mainly using density functional theory (DFT) or ab initio calculations. Figure 6 shows that there is a band gap between VB and CB. According to ligand field theory, as Ti (or Ni) centers the TiO_6 (or NiO_6) octahedron in the crystal, the Ti 3*d* or (Ni 3*d*) orbitals split into t_{2g} and, e.g., orbitals. The 3*d* orbitals of metal ions bond with the O 2*p* orbitals and then form the energy bands.

As a typical photocatalyst, nanosized TiO_2 (anatase or rutile) has an experimental band gap of 3.1–3.3 V [26]. TiO_2 consists of TiO_6 octahedra. The calculated DOSs are illustrated as Fig. 6a [39–42]. Both VB and CB consist of the hybridized O 2*p* and Ti 3*d* orbitals. Nevertheless, the VB is predominately formed from O 2*p* orbitals, and the CB from Ti 3*d* orbitals. At the bottom of CB, the high DOSs peak originates from the dominative Ti 3*d* (t_{2g}^*) antibonding with less O 2p orbitals. Obviously, the electrons in Ti 3*d* orbitals more often occupy the t_{2g}^* orbitals than the low energy levels, e.g., and t_{2g} orbitals.

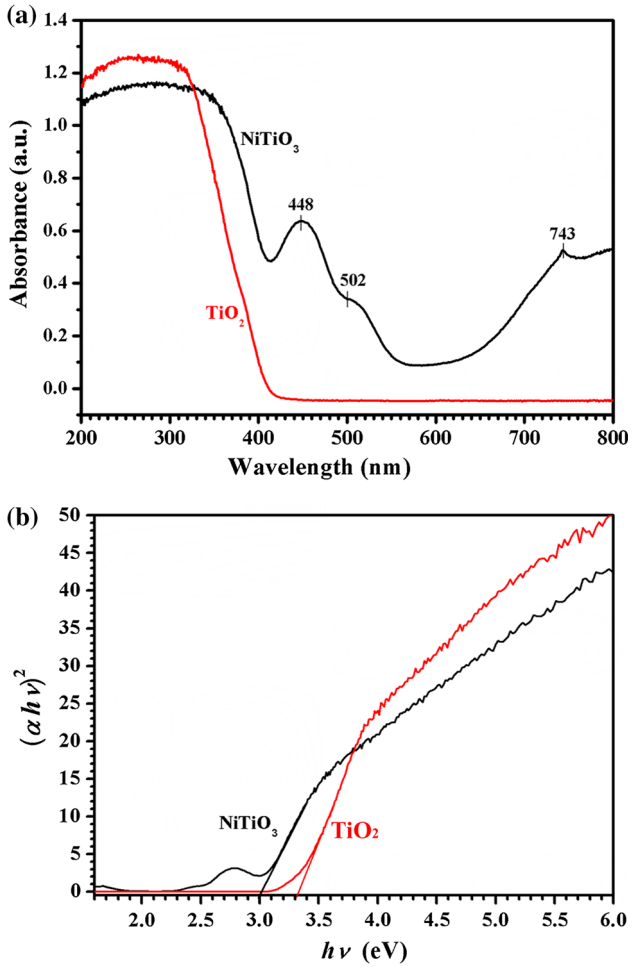

Fig. 4 **a** UV–Vis DRS of the synthetic $NiTiO_3$ and Degussa P-25 at room temperature and **b** Tauc plots obtained from the UV–Vis DRS

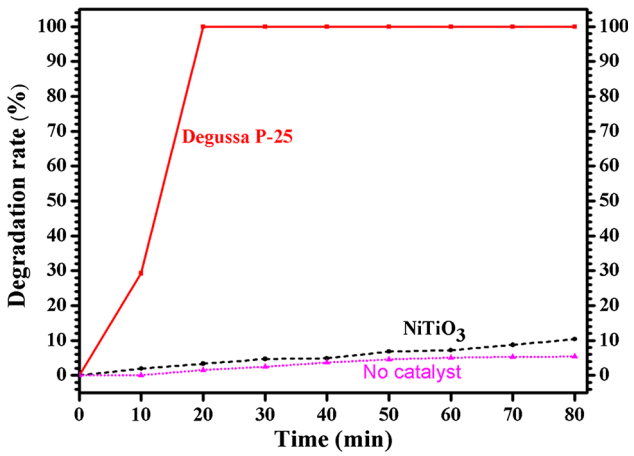

Fig. 5 Photocatalytic performance of $NiTiO_3$ and Degussa P-25 in the degradation of methylene blue in water. A sample without catalyst is detected as reference

Umebayashi et al. [39] pointed out that the location of t_{2g}^* determines the photoexcitation of TiO_2, and the dopant t_{2g} level in the band gap plays a vital role for the visible light response of TiO_2. Experimentally, Degussa P-25 hardly absorbs visible light, but exhibits nice photocatalytic activity under UV light. The most charge-transfer transitions in TiO_2 should occur between O 2*p* and Ti 3*d* (t_{2g}^*), i.e., $O^{2-} \rightarrow Ti^{4+}$, under UV light.

Figure 6b shows that NiO has a wide band gap of 3.7–4.3 eV [43, 44] and generally is considered as an insulating material. NiO consists of NiO_6 octahedra. Its both VB and CB are predominately from Ni 3*d* orbitals [43–46]. Most DOSs of Ni 3*d* locate within the VB. The wide energy gap between the nearby DOSs peaks of CB and VB blocks the charge-transfer transitions by either Ni 3*d* (t_{2g}^*) → Ni 2*d* (e.g., *) or O 2*p* → Ni 3*d* (e.g., *). NiO (at 300 °C) shows optical absorption lines at 1.13, 1.75, 2.75, and 2.95 eV [47], which should mainly originate from the Ni: *d* → *d* transitions with low energy gaps in the VB after absorbing visible light.

Compared with TiO_2 and NiO, $NiTiO_3$ has a more complicated band structure due to its alternating layers of NiO_6 and TiO_6 octahedra. Its band structure is schematically shown in Fig. 6c. Ruiz-Preciado et al. [37] argued that the bulk $NiTiO_3$ has a band gap of ~2.55 eV between the DOSs of Ni 3*d* and O 2*p* but with relatively low mobility of charges. The VB of $NiTiO_3$ mainly derives from the hybridization of Ni 3*d* and O 2*p* orbitals; while the CB predominately consists of Ti 3*d* orbitals. Being similar to the case of NiO, most Ni 3*d* orbitals in $NiTiO_3$ locate in the VB. The observed absorbance peaks at 1.67, 2.47, and 2.77 eV should be caused by the Ni: *d* → *d* transitions in the VB. The wide energy gap (>5.5 eV) from the hybridized Ni 3d (t_{2g}^*) and O 2*p* orbital peak to the predominated Ti 3*d* orbital peak in CB baffles the charge-transfer transitions by both Ni 3*d* → Ti 3*d* and O 2*p* → Ti 3*d* transitions under visible light.

Ruiz-Preciado et al. [37] argued that the band gap and optical properties of $NiTiO_3$ could be modified by the size of $(NiTiO_3)_n$ nanoclusters or the surface roughness (~19 nm) of $NiTiO_3$ thin films [25]. They suggested that the photocatalytic efficiency of $NiTiO_3$ may be improved by a doping procedure to increase the concentration of photogenerated charge carriers and their lifetime.

In summary, $NiTiO_3$ has a narrower band gap than TiO_2 and also selectively absorbs visible light. Nevertheless, $NiTiO_3$ has a crystal structure consisting of alternating NiO_6 and TiO_6 layers and induces a wide energy gap from the hybridized Ni 3*d* and O 2*p* orbitals to the predominated Ti 3*d* orbitals, which blocks both $Ni^{2+} \rightarrow Ti^{4+}$ and O 2*p* → Ti 3*d* charge-transfer transitions. These baffle the

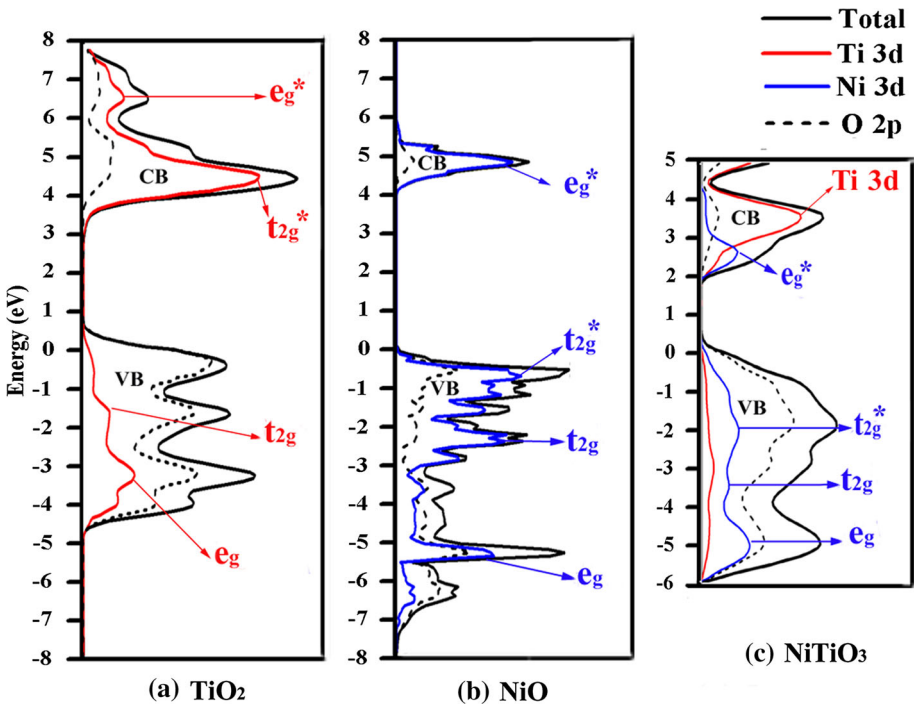

Fig. 6 Schematic energy bands and density of states (DOSs) for TiO_2 (anatase), NiO, and $NiTiO_3$. The data for the *curves* are taken from literature [40, 43], and [37], respectively

photocatalytic performance of $NiTiO_3$. The yellow color of $NiTiO_3$ originates from its selective absorption of visible light and reflects the Ni: $d \rightarrow d$ charge-transfer transitions occurring in the valence band.

4 Conclusions

We synthesized $NiTiO_3$ nanocrystallites via a solid-state reaction after the precursor being prepared by a homogeneous precipitation method. The nanosized $NiTiO_3$ is a direct-gap semiconducting material with a band gap of 3.00 eV. It selectively absorbs visible light at 448, 502, and 743 nm. The stable wavelengths of the absorption peaks imply that they originate from the Ni: $d \rightarrow d$ charge-transfer transitions within the valence band. The $NiTiO_3$ nanoparticles do not exhibit obvious photocatalytic activity as being used in degrading methylene blue. The mixed octahedron layer crystal structure and the wide energy gap are two suggested factors which affect the photocatalytic activity of $NiTiO_3$.

References

1. Y. Ishikawa, S. Sawada, J. Phys. Soc. Jpn. **11**, 496 (1956)
2. R.S. Singh, T.H. Ansari, R.A. Singh, B.M. Wanklyn, Mater. Chem. Phys. **40**, 173 (1995)
3. L. Zhou, S.-Y. Zhang, J.-C. Cheng, L.-D. Zhang, Z. Zeng, Mater. Sci. Eng. B **49**, 117 (1997)
4. Y.-J. Lin, Y.-H. Chang, W.-D. Yang, B.-S. Tsai, J. Non-Cryst. Solids **352**, 789 (2006)
5. S.-H. Chuang, M.-L. Hsieh, D.-Y. Wang, J. Chin. Chem. Soc. **59**, 628 (2012)
6. C. Xin, Y. Wang, Y. Sui, Y. Wang, X. Wang, K. Zhao, Z. Liu, B. Li, X. Liu, J. Alloys Compd. **613**, 401 (2014)
7. S. Moghiminia, H. Farsi, H. Raissi, Electrochim. Acta **132**, 512 (2014)
8. T. Acharya, R.N.P. Choudhary, J. Eelectron. Mater. **44**, 271 (2015)
9. G.R. Rossman, R.D. Shannon, R.K. Waring, J. Solid State Chem. **39**, 277 (1981)
10. I.V. Pishch, E.V. Radion, Glass Ceram. **60**, 154 (2003)
11. R. Levinson, P. Berdahl, H. Akbari, Sol. Energy Mater. Sol. Cells **89**, 351 (2005)
12. J.-L. Wang, Y.-Q. Li, Y.-J. Byon, S.-G. Mei, G.-L. Zhang, Powder Technol. **235**, 303 (2013)
13. Y. Tong, J. Fu, Z. Chen, J. Nanomater. **2016**, 5464978 (2016)
14. P. Salvador, C. Gutierrez, J.B. Goodenough, Appl. Phys. Lett. **40**, 188 (1982)
15. P. Salvador, C. Gutiérrez, J.B. Goodenough, J. Appl. Phys. **53**, 7003 (1982)
16. P.H.M. de Korte, G. Blasse, J. Solid State Chem. **44**, 150 (1982)
17. L.G.J. de Haart, A.J. de Vries, G. Blasse, Mater. Res. Bull. **19**, 817 (1984)
18. X. Shu, J. He, D. Chen, Ind. Eng. Chem. Res. **47**, 4750 (2008)
19. Y.-J. Lin, Y.-H. Chang, G.-J. Chen, Y.-S. Chang, Y.-C. Chang, J. Alloys Compd. **479**, 785 (2009)
20. M.S. Sadjadi, M. Mozaffari, M. Enhessari, K. Zare, Superlattice Microst. **47**, 685 (2010)
21. K.S. Beenakumari, J. Exp. Nanosci. **8**, 203 (2013)
22. P. Yuan, C. Fan, G. Ding, Y. Wang, X. Zhang, Int. J. Miner. Metall. Mater. **19**, 372 (2012)
23. Y. Qu, W. Zhou, Z. Ren, S. Du, X. Meng, G. Tian, K. Pan, G. Wang, H. Fu, J. Mater. Chem. **22**, 16471 (2012)
24. A. Sobhani-Nasab, S.M. Hosseinpour-Mashkani, M. Salavati-Niasari, H. Taqriri, S. Bagheri, K. Saberyan, J. Mater. Sci. Mater. Electron. **26**, 5735 (2015)

25. M.A. Ruiz-Preciado, A. Bulou, M. Makowska-Janusik, A. Gibaud, A. Morales-Acevedo, A. Kassiba, CrystEngComm **18**, 3229 (2016)
26. A.L. Linsebigler, G. Lu, J.T. Yates, Chem. Rev. **95**, 735 (1995)
27. R. Asahi, T. Morikawa, T. Ohwaki, K. Aoki, Y. Taga, Science **293**, 269 (2001)
28. K.P. Lopes, L.S. Cavalcante, A.Z. Simões, J.A. Varela, E. Longo, E.R. Leite, J. Alloys Compd. **468**, 327 (2009)
29. E. Matijević, Chem. Mater. **5**, 412 (1993)
30. X.M. Gao, M.W. Li, Y.L. Hou, C.Y. Wang, Mater. Res. Innov. **19**, 1 (2015)
31. C.R. Hubbard, E.H. Evans, D.K. Smith, J. Appl. Cryst. **9**, 169 (1976)
32. K.T. Jacob, V.S. Saji, S.N.S. Reddy, J. Chem. Thermodyn. **39**, 230 (2007)
33. D.H. Kim, H.S. Park, S.-J. Kim, K.S. Lee, Catal. Lett. **106**, 29 (2006)
34. J. Tauc, R. Grigorovici, A. Vancu, Phys. Status Solidi **15**, 627 (1966)
35. M.A. Ruiz-Preciado, A. Kassiba, A. Gibaud, A. Morales-Acevedo, Mater. Sci. Semicond. Proc. **37**, 171 (2015)
36. R. Vijayalakshmi, V. Rajendran, E. J. Chem. **9**, 282 (2012)
37. M.A. Ruiz Preciado, A. Kassiba, A. Morales-Acevedo, M. Makowska-Janusik, RSC Adv. **5**, 17396 (2015)
38. N. Pal, B. Saha, S.K. Kundu, A. Bhaumik, S. Banerjee, New J. Chem. **39**, 8035 (2015)
39. T. Umebayashi, T. Yamaki, H. Itoh, K. Asai, J. Phys. Chem. Solids **63**, 1909 (2002)
40. F. Tian, C.B. Liu, J. Phys. Chem. B **110**, 17866 (2006)
41. N. Martsinovich, D.R. Jones, A. Troisi, J. Phys. Chem. C **114**, 22659 (2010)
42. H.Y. Lee, J. Robertson, J. Appl. Phys. **113**, 213706 (2013)
43. X.-B. Feng, N.M. Harrison, Phys. Rev. B **69**, 035114 (2004)
44. F. Tran, P. Blaha, Phys. Rev. Lett. **102**, 226401 (2009)
45. G.A. Sawatzky, J.W. Allen, Phys. Rev. Lett. **53**, 2339 (1984)
46. R. Gillen, J. Robertson, J. Phys. Condens. Matter **25**, 165502 (2013)
47. R. Newman, M. Chrenko, Phys. Rev. **114**, 1507 (1959)